PHYSICAL REVIEW E **70**, 050601(R) (2004)

Observation of a two-step mechanism in the formation of a superstructure of cadmium-behenic acid Langmuir monolayer: Evidence of an intermediate structure

S. Cantin, J. Pignat, and F. Perrot
LPPI (EA 528), Université de Cergy-Pontoise, Neuville sur Oise, 95 031 Cergy-Pontoise Cedex, France

P. Fontaine and M. Goldmann
LURE (UMR CNRS 130), Centre Universitaire Paris Sud, Boîte Postale 34, 91 898 Orsay Cedex and GPS (UMR CNRS 75-88), Universités Paris VI et VII, France

(Received 8 March 2004; published 11 November 2004)

By means of grazing incidence x-ray diffraction, the structure of a behenic acid monolayer spread over chloride salt solutions of cadmium is observed to evolve from the tilted L_2 phase to the superstructure (corresponding to an organized monolayer of ions in addition to the ordered organic film), through an intermediate phase. The studied salt concentrations are below the so-called "threshold" needed for the formation of this superstructure. This kinetic process involving two first-order phase transitions is confirmed by Brewster angle microscopy experiments and surface pressure-area isotherms measured at different times after monolayer deposition.

DOI: 10.1103/PhysRevE.70.050601 PACS number(s): 68.18.Jk, 61.10.Nz, 68.37.−d

Understanding the growth mechanisms of a mineral layer directed by an organic matrix is of great importance for the design of biomimetic composite materials [1]. Several studies investigate the nanoarchitecture and mechanical properties of natural organic-inorganic assemblies, such as nacre [2–4]. Simultaneously, model systems have been developed for testing biomineralization processes [5–9]. Among them, monolayers of amphiphilic molecules (Langmuir monolayers) at the interface of air-aqueous solutions of metal ions allow a systematic study of the mechanisms of surfactant-mediated nucleation of the inorganic layer. This approach provides the possibility of tuning easily the experimental parameters (choice of the organic and inorganic components, *p*H and subphase concentration…). Moreover, well-adapted experimental techniques, such as grazing incidence x-ray diffraction (GIXD), are now available to characterize the film structure. Experiments on mineralization driven by Langmuir monolayer templates have been performed from either supersaturated or dilute salt solutions of divalent cations. In the first case, many works focus on the growth of oriented crystals of specific morphology [10–12]; recent *in situ* structural studies have investigated the commensuration between the lattices of the organic monolayer and the mineral [7–9]. For dilute salt solutions and fatty acid monolayers as organic templates, superlattice structures have been evidenced in the case of chloride salts of cadmium, lead, manganese, and magnesium [13–16]. The superlattice corresponds to an organized monolayer of cations complexes below the well-ordered organic monolayer. In a recent work [16], for these four cations, a threshold of subphase concentration was demonstrated for the superlattice formation, by means of surface pressure-area isotherms and GIXD measurements. Below the threshold, the cations have just a condensing effect on the organic layer, as it is observed, at any concentration, for chloride salts of zinc, barium, nickel, cobalt, or copper [15]. The mechanisms of formation of the superlattice, its chemical composition, as well as the reasons why only some cations lead to superstructures, are still unknown.

In this Rapid Communication, we have investigated behenic acid (BA) Langmuir monolayers spread over chloride salt solutions of cadmium ($CdCl_2$) below the threshold evidenced for the superstructure formation. Brewster angle microscopy (BAM) experiments, carried out with monolayers deposited at lower molecular areas than in our previous work [16], revealed a kinetic effect below the threshold. Then, the film structure is analyzed as a function of time by means of GIXD and correlated to BAM observations of the changes in monolayer texture on a macroscopic scale (>1 μm). Eventually, the kinetic study of surface pressure-area isotherms are used to confirm BAM and GIXD. In order to perform this kinetic study, a well-adapted GIXD device was necessary. Although third generation synchrotron sources allow to follow fast evolutions, degradations of the films induced by the strong brilliance of the incident beam are quickly observed in the case of cadmium (Cd) superstructures. To avoid these drawbacks, we took advantage of a set up using a two-dimensional (2D) detector reducing the acquisition time up to a few minutes with a less intense first generation synchrotron source (DCI at LURE) [17].

Behenic acid and cadmium chloride were purchased from Sigma. The *p*H was adjusted to 7.5 by the addition of $NaHCO_3$ (Sigma). The experiments were performed at room temperature (20 °C). Various Langmuir troughs of different geometries (area/volume ratios) were used. The time scale of the evolutions was reproducible from one trough to another provided that the Cd concentration was expressed as a number of Cd ions per BA molecule. Isotherm measurements were performed on a 601BAM Langmuir–Blodgett trough from Nima. The GIXD experiments were carried out at the LURE synchrotron source on the D41B beam line. The selected wavelength was 1.605 Å. The angle of incidence α of the x-ray beam was fixed to $0.85\alpha_c$, where α_c=2.4 mrad is the critical angle for total internal reflection for water. To monitor the diffracted intensity as a function of the in-plane component Q_{xy} and vertical component Q_z of the scattering vector, a thin vertical slit was placed between the trough and the 2D detector. The horizontal gap of the slit was 1 mm. The sample-slit and the sample-detector distances were, respectively, 220 and 600 mm, leading to a maximum Q_{xy} resolution of $0.1\ \mathrm{nm}^{-1}$. The acquisition time of each scan was 5 mins. BAM [18,19] takes advantage of the properties of reflectivity of an interface illuminated at the Brewster angle with light polarized in the plane of incidence. First-order phase transitions can be visualized in this way. Moreover, with an analyzer placed in the path of the reflected light, optical anisotropies due to the molecular tilt [20,21] or to the unit-cell anisotropy in untilted phases [20,22] can be detected. On the images, each shade of gray corresponds either to a different tilt-azimuthal orientation of the molecules in the tilted phases or to a different orientation of the unit cell in the untilted phase.

We have investigated the time evolution of BA monolayers spread at zero surface pressure and molecular area $A = 23\ \text{Å}^2$ over $CdCl_2$ solutions adjusted at pH 7.5. Two experimental parameters were observed to influence the time scale of the evidenced kinetic effect but the sequence of phases remains unchanged. First, the process is all the more fast as the Cd concentration is close to the threshold for superstructure formation (3.5 Cd ions per BA molecule). Second, the evolutions are slower at larger molecular area, i.e., increasing the gaseous phase area. This explains why no kinetic effect has been detected in the experiments performed at initial molecular areas between 36 and 51 Å^2 [16]. In the following, we describe the results for a salt concentration of 2 Cd ions per BA molecule (i.e., 6.3×10^{-7} mol/l in GIXD experiments). We report the evolution of the diffraction pattern for Q_{xy} in the range $1.35-1.7\ \text{Å}^{-1}$ and the associated BAM observations. The process can be divided into five stages.

Stage 1 (from $t=0$ to 80 min): Just after monolayer deposition, as already reported [16], GIXD data indicate the presence of two lower-order diffraction peaks corresponding to BA molecules in the L_{2h} phase. In the centered rectangular cell, the in-plane peak observed at lower Q_{xy} is the (02) peak, whereas the out-of-plane peak is the degenerate (11) and $(1\overline{1})$ Bragg reflection. The molecules are tilted towards a nearest neighbor with an angle of about 23° with respect to the surface normal. With BAM, the film looks like a BA monolayer over pure water at zero surface pressure and $A = 23\ \text{Å}^2$ [21]. Without analyzer, large bright domains of the L_{2h} phase coexist with small dark patches of gas. With analyzer, the L_{2h} domains are divided into regions of different shade of gray corresponding to different tilt-azimuthal orientations of the molecules [Fig. 1(a)]. Until $t=80$ min, one observes a continuous decrease of the tilt angle of the molecules down to 14.5°. Indeed, the Q_z component of the $(11)/(1\overline{1})$ peak as the Q_{xy} one shifts towards higher values. With BAM, this evolution manifests itself by a slight decrease of contrast between the regions of different tilt-azimuthal directions [Fig. 1(b)].

Stage 2 (from $t=80$ to 100 min): A new diffraction peak is detected in addition to the two Bragg reflections corresponding to the L_{2h} phase [Fig. 2(a)]. This broad in-plane peak is measured at the same Q_{xy} position ($1.519\ \text{Å}^{-1}$) as the $(11)/(1\overline{1})L_{2h}$ phase out-of-plane peak. Figure 2(b) shows the

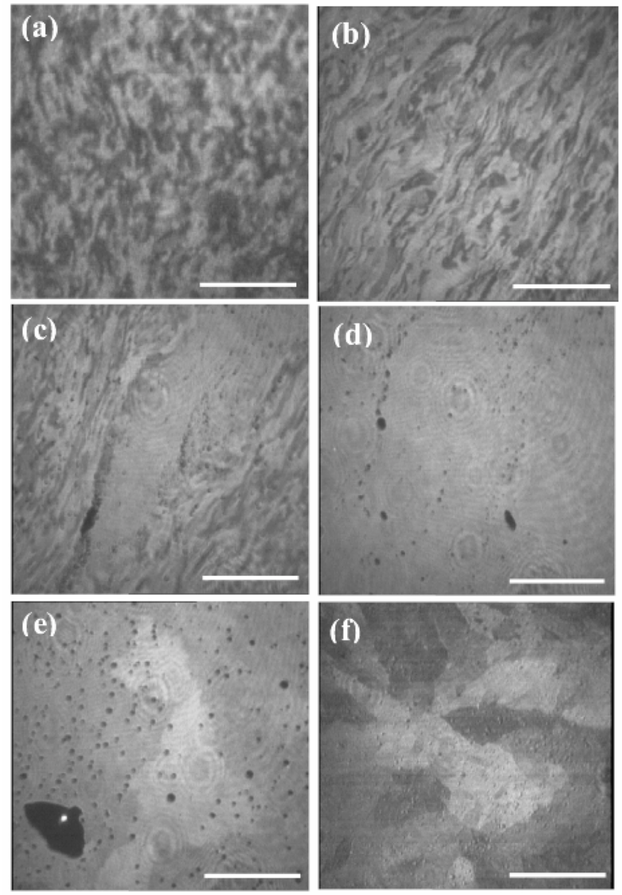

FIG. 1. BAM images with an analyzer for a BA monolayer spread over $CdCl_2$ (2 Cd ions / BA molecule, pH 7.5), as a function of resting time after film deposition: (a) $t=10$ min, L_{2h} phase; (b) $t=70$ min, L_{2h} phase; (c) $t=85$ min, L_{2h}/I coexistence; (d) $t=110$ min, I phase; (e) $t=185$ min, I/superstructures coexistence; (f) $t=210$ min, superstructures. The white bar represents 200 μm.

Bragg rod at $Q_{xy}=1.519\ \text{Å}^{-1}$, which allows to distinguish between the two peaks. The broad in-plane peak indicates a short-range organization of straight BA molecules in a hexagonal lattice. The rectangular cell parameters deduced from the peak position are $a=4.79$ Å and $b=8.30$ Å. By fitting this peak with a Lorentzian shape, one obtains its full width at half maximum (FWHM) leading to a positional correlation length $L\,[L=2(\mathrm{FWHM})]$ close to 30 Å, about eight molecules. As long as the three diffraction peaks are detected, their positions remain fixed and the intensity of the L_{2h} phase peaks decreases to the advantage of that of the broad peak. It means that a first-order phase transition takes place between the L_{2h} phase and a weakly ordered intermediate phase called the "I phase" in the following. This transition is confirmed by BAM. Indeed, with analyzer, the nucleation of optically isotropic patches is observed in the condensed domains. Figure 1(c) shows a domain in which regions of the L_{2h} phase coexist with an isotropic zone in agreement with the I phase hexagonal packing. As expected for a first-order phase transition, the surface covered by the L_{2h} phase decreases until the domains appear completely optically isotropic, i.e., in the I phase [Fig. 1(d)].

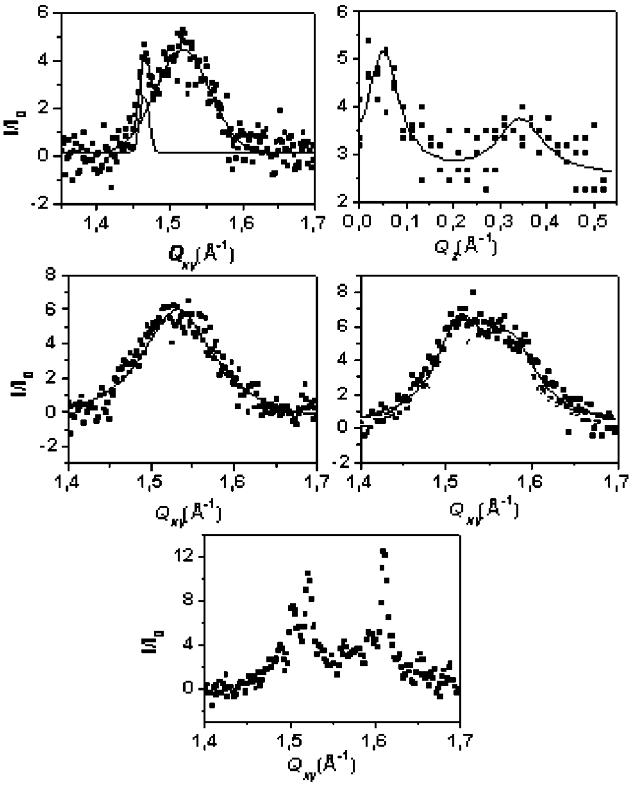

FIG. 2. GIXD data in the horizontal plane [except (b)] integrated over Q_z for a BA monolayer over $CdCl_2$ (2 Cd ions/BA molecule, *p*H 7.5), as a function of resting time after film deposition: (a) $t=95$ min, L_{2h}/I coexistence; the Bragg rod at $Q_{xy}=1.519$ Å^{-1} (b) allows to distinguish between the out-of-plane L_{2h} phase peak and the *I* phase peak; (c) $t=105$ min, *I* phase; (d) $t=125$ min, *I* phase; (e) $t=175$ min, *I*/superstructures coexistence.

Stage 3 (from $t=100$ to 160 min): At $t=100$ min, the two L_{2h} phase diffraction peaks are no longer detectable and only the *I* phase broad in-plane peak is observed. Figures 2(c) and 2(d) show the diffraction patterns obtained, respectively, at $t=105$ and 125 min. Until $t=110$ min, the same peak is observed with a slight continuous shift of its position towards higher Q_{xy} as a function of time. Then, from $t=110-160$ min, the shape of the in-plane peak is no longer symmetrical indicating a slight distortion of the hexagonal lattice. However, the organization of the BA molecules remains short ranged. The diffraction pattern looks like the rotator *I* phase observed in heneicosanoïc acid monolayers over pure water [23]. By means of BAM with analyzer, the condensed domains appear optically isotropic [Fig. 1(d)]. The slight lattice anisotropy is not detected, probably because of a too-weak molecular arrangement.

Stage 4 (from $t=160$ to 190 min): The GIXD patterns reveal in the studied Q_{xy} range the presence of three resolution-limited out-of-plane peaks, in addition to the *I* phase asymmetrical broad in-plane peak [Fig. 2(e)]. The position of these three peaks is exactly the same as that detected in the case of superstructures [16]. These peaks correspond to the arrangement of tilted BA molecules in a pseudorectangular cell. The two Cd superlattice peaks that should be observed at 1.41 and 1.58 Å^{-1} are not detected, certainly due to their weak intensities associated to the superposition of the *I* phase peak. The three characteristic peaks of the superstructure, as well as the *I* phase peak, are locked at the same positions during all this period. Only the *I* phase peak intensity decreases to the advantage of the superstructure peaks one. It indicates a coexistence between superstructures and the *I* phase, i.e., a second first-order phase transition. By means of BAM with analyzer, the beginning of this stage is marked by the appearance in the condensed domains of patches with regions of different shades of gray [Fig. 1(e)]. This optical anisotropy is in agreement with the nucleation of the tilted superstructure phase evidenced by GIXD. One can notice that the regions of different tilt-azimuthal orientations are much larger than those observed in the L_{2h} phase. With time, the optically anisotropic patches grow in size until the isotropic zones corresponding to the *I* phase disappear completely. These observations are consistent with GIXD data and confirm a first-order phase transition between the *I* phase and the superlattice structure.

Stage 5 (after $t=190$ min): GIXD reveals the same diffraction pattern as that obtained in [16] above the concentration threshold for superstructure formation. The film has thus evolved towards the superlattice structure by means of two first-order phase transitions. Figure 1(f) is a BAM image showing a condensed domain observed at this stage with an analyzer. Regions with different shades of gray are visualized. This is in agreement with tilted BA molecules in the superstructure phase. We have checked that the observed texture is similar to that visualized above the concentration threshold.

Figure 3(a) shows the time evolution of the cell parameters *a* and *b* deduced from the diffraction patterns. To discriminate between the two possible indexations of the *I* phase asymmetrical peak, the cell parameters obtained in the two cases were compared with those measured both in the *I* phase for the symmetrical peak and in the superstructure phase. One deduced that the lower Q_{xy} peak corresponds to the degenerate $(11)/(1\overline{1})$ peak and the other one to the (02) Bragg reflection, as in the *S* phase of fatty acid monolayers. Using a,b, and the tilt angle, we have also calculated the parameters a_T and b_T of the transverse cell obtained by projection of the (a,b) cell onto a plane normal to the long axis of the molecules. This transverse cell is represented in Fig. 3(b) at different stages of the evolution. At the L_{2h}-*I* phase transition, both a_T and b_T change. Then, one can notice that the parameter b_T decreases continuously during the *I* phase and jumps to a lower value in the superlattice phase. In contrast, the parameter a_T has already reached its superstructure value at the beginning of the *I* phase. This probably indicates a crystallization direction along the parameter *a* in the *I* phase. However, we do not succeed to detect the higher-order (20) peak that should be resolution limited. From the cell parameters *a* and *b*, one can also calculate the mean molecular area *A*. A strong lattice contraction is observed between the beginning of the L_{2h} phase ($A=21.3$ Å^2) and the superstructure ($A=19.2$ Å^2). One can notice that this reduction in molecular area manifests itself on BAM images by the nucleation in the dense domains of small hollows of gas

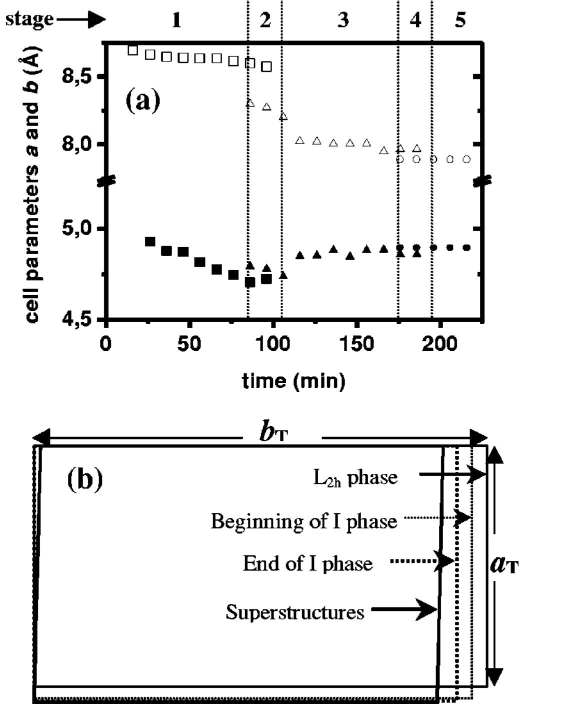

FIG. 3. (a) Evolution with time of the rectangular cell parameters a (full symbol) and b (empty symbol), for a BA monolayer over $CdCl_2$ (2 Cd ions/BA molecule, pH 7.5). The five stages are indicated. Squares: L_{2h} phase; triangles: I phase; circles: superstructures. (b) Schematic representation of the rectangular transverse cell at different stages.

[Fig. 1]. Their area fraction is compatible with the decrease in A.

In order to confirm GIXD and BAM experiments, isotherms were also measured at different times after monolayer deposition. Figure 4 presents the results obtained for a BA monolayer spread at an area $A=27$ Å^2 over $CdCl_2$ (2 ions/BA molecule). Each isotherm was monitored in 5 min. One can notice that the isotherm's shape varies strongly as a function of time. The first isotherm, measured just after monolayer spreading, presents the same phase transitions as over pure water but is shifted towards a lower molecular area, indicating a condensing effect of Cd ions. At longer times, the L_{2h}-L_2' and L_2'-S transitions are no longer visible. The basic point is that, at the end of the evolution ($t=275$ min), the isotherm is similar to that obtained in [16] above the Cd concentration threshold for superstructure formation. This observation is thus in agreement with the superlattice structure evidenced at this stage by means of GIXD.

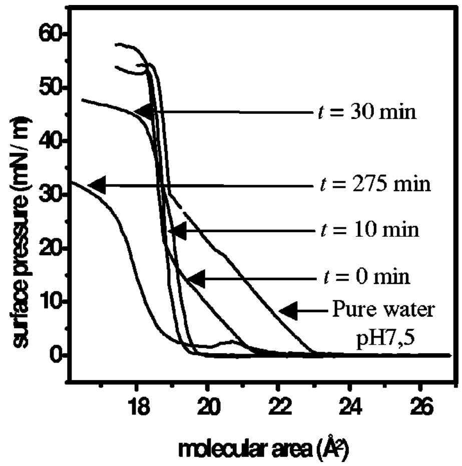

FIG. 4. Isotherms for a BA monolayer over $CdCl_2$ (2 Cd ions/BA molecule, pH 7.5), as a function of resting time after film deposition, compared to the isotherm over pure water adjusted to pH 7.5.

In conclusion, we evidenced, in BA monolayers spread over $CdCl_2$ solutions adjusted at pH 7.5, that the initial L_{2h} phase evolves to the superstructure via an intermediate phase, I, through two successive first-order transitions. We observed that the crystallization of the organic lattice begins in the I phase, along the parameter a of the rectangular cell. Such an experiment was successful by monitoring the structure evolution with the 2D detector set up. A good agreement is obtained with BAM and isotherms measurements. The sequence of phases is independent of the ion concentration, except in terms of time scale. This indicates that the so-called threshold is not a real physical parameter but just a quantity of ions above which the kinetic formation is too fast to be followed. Further experiments are in progress regarding both the other cations and the chemical nature and organization of the inorganic lattice.

[1] Z. Tang, N. A. Kotov *et al.*, Nat. Mater. **2**, 413 (2003).
[2] F. Song, A. K. Soh *et al.*, Biomaterials **24**, 3623 (2003).
[3] S. Weiner and W. Traub, FEBS Lett. **111**, 311 (1980).
[4] B. L. Smith *et al.*, Nature (London) **399**, 761 (1999).
[5] P. Kjellin *et al.*, Langmuir **19**, 9196 (2003).
[6] E. DiMasi *et al.*, Langmuir **18**, 8902 (2002).
[7] J. Kmetko *et al.*, Phys. Rev. Lett. **89**, 186102 (2002).
[8] I. Weissbuch *et al.*, Cryst. Growth Des. **3**, 125 (2003).
[9] J. Kmetko *et al.*, Phys. Rev. B **68**, 085415 (2003).
[10] B. R. Heywood and S. Mann, Langmuir **8**, 1492 (1992).
[11] B. Li *et al.*, Langmuir **15**, 4837 (1999).
[12] L. Lu *et al.*, Chem. Mater. **13**, 325 (2001).
[13] F. Leveiller, *et al.*, Langmuir **10**, 819 (1994).
[14] J. Kmetko *et al.*, Langmuir **17**, 4697 (2001).
[15] J. Kmetko *et al.*, J. Phys. Chem. B **105**, 10818 (2001).
[16] V. Dupres *et al.*, Langmuir **19**, 10808 (2003).
[17] P. Fontaine *et al.*, Rev. Sci. Instrum. (to be published).
[18] S. Hénon and J. Meunier, Langmuir **62**, 936 (1991).
[19] D. Hönig and D. Möbius, J. Phys. Chem. **95**, 4590 (1991).
[20] S. Rivière *et al.*, J. Chem. Phys. **101**, 10045 (1994).
[21] S. Rivière-Cantin *et al.*, Phys. Rev. E **54**, 1683 (1996).
[22] G. A. Overbeck *et al.*, Thin Solid Films **242**, 26 (1994).
[23] M. C. Shih *et al.*, Phys. Rev. A **45**, 5734 (1992).